DEUTSCHES ELEKTRONEN-SYNCHROTRON DESY

DESY SR 84-21
September 1984

RESONANT SATELLITE PHOTOEMISSION OF ATOMIC Mn

by

E. Schmidt, H. Schröder, B. Sonntag, H. Voss and H.E. Wetzel

II. Institut f. Experimentalphysik, Universität Hamburg

ISSN 0723-7979

NOTKESTRASSE 85 · 2 HAMBURG 52

To be sure that your preprints are promptly included in the
HIGH ENERGY PHYSICS INDEX ,
send them to the following address (if possible by air mail) :

DESY
Bibliothek
Notkestrasse 85
2 Hamburg 52
Germany

DESY SR 84-21
September 1984

ISSN 0723 - 7979

Resonant satellite photoemission of atomic Mn

E. Schmidt, H. Schröder, B. Sonntag, H. Voss
and H.E. Wetzel

II. Institut für Experimentalphysik
der Universität Hamburg, Hamburg, Germany

The photoelectron spectra and the relative partial photoionization cross sections of atomic Mn have been determined for photon energies between 45 eV and 65 eV. Besides the main $3d^5 4s^2\ ^6S \rightarrow 3d^4 4s^2(^5D)\varepsilon l$, $3d^5 4s(^{5,7}S)\varepsilon l$ photoemission lines there are prominent $3d^4 4s\ n l \varepsilon l$ satellite photoemission lines which are strongly enhanced in the range of the giant $3p \rightarrow 3d$ resonance and the $3p^6 3d^5 4s^2 \rightarrow 3p^5 3d^5 4s^2 nl$ Rydberg transitions. Near the 3p - 3d resonance the partial cross sections of these two electron satellites behave similar to that of the $3d^5 4s^2 \rightarrow 3d^4 4s^2 \varepsilon l$ main line. The interference between the $3p^6 3d^5 4s^2\ ^6S \rightarrow 3p^5 3d^6 4s^2\ ^6P$ excitation and the continuum channels manifests itself in the asymmetric profiles of the partial cross sections. In contrast to this, the $3d^5 4s^2 \rightarrow 3d^5 4s\ ^5L\ \varepsilon l$ partial cross sections can be approximated by the superposition of Lorentzians centered at the $3p^6 3d^5 4s^2\ ^6S \rightarrow 3p^5 3d^6 4s^2\ ^6D, ^6P, ^4L$ excitation energies. The $3d^5 5s \varepsilon l$ photoemission only undergoes a single symmetric resonance. All these lines including the main lines do not show an enhancement close to the $3p^5 3d^5 4s^2\ ^7P$ ionization limits. When tuning the photon energy across these ionization limits, post collision interactions give rise to further satellite lines, and to asymmetric $M_{2,3} M_{4,5} N_1$ Auger lines which, in comparison to the normal Auger lines, are shifted towards higher energies.

to be published in J. of Phys. B ... (1984)

I. Introduction

Many electron effects result in strong deviations from the independent particle model for atoms with filled and empty orbitals with similar spatial dimensions (Wendin 1982a,b; Starace 1982; Samson 1982; Crasemann and Wuilleumier 1984; Amusia 1983; Kelly 1983; Zangwill 1983). The large overlap of the 3p and 3d orbitals makes the atomic 3d transition metals excellent examples. The strong coupling of the $3p \rightarrow 3d$ and $3d \rightarrow \varepsilon f$ excitations results in a resonant enhancement of the 3d photoemission lines (Bruhn et al. 1982a,b; Schmidt et al. 1983; Kobrin et al. 1984; Krause et al. 1984). The gross features of the photoemission spectra are in agreement with model calculations performed by Davis and Feldkamp (1976, 1978, 1983). A more detailed analysis requires the extension of the methods developed for treating electron correlation to the treatment of atoms with partly filled shells. Despite the success of various methods for closed shell atoms (Wendin 1982a,b; Starace 1982; Amusia 1983; Kelly 1983; Zangwill 1983) only a few attempts have been undertaken to tackle the spectra of open shell atoms (Kelly 1983; Amusia 1983; Zangwill 1983; Combet-Farnoux 1980; Garvin et al. 1983, 1984; Amusia et al. 1981a,b, 1983). The main problem rests with the great number of interacting open and closed channels.

The complexity is reduced for almost empty, almost filled and for half filled shells. Atoms with half filled shells occupy an intermediate position between closed shell atoms and open shell atoms. This greatly facilitates the extension of the existing theoretical approaches to these atoms. Atomic Mn, which has a $3p^6 3d^5 4s^2\ ^6S$ ground state configuration of the outer shells, therefore forms an ideal testing ground. The characteristic features of the absorption and photoemission spectra of atomic Mn for photon energies close to the 3p threshold are well described by model calculations based on the extension of Fano's theory (Fano 1961) to the case of many discrete states interacting with many continua (Davis and Feldkamp 1977, 1978, 1981; Bruhn et al. 1978, 1982a). Improved agreement with the experimental profile of the giant photoionization resonance at the 3p threshold has been achieved by Amusia et al. (1981). By dividing each atomic subshell, except the half filled one, into two subshells, in each of which all electron spins are parallel they constructed a quasi closed shell system to which the closed-shell RPAE formalism could be applied. Spin-orbit interaction was not taken into account. Therefore the sharp $3p^6 3d^5 4s^2\ ^2S \rightarrow 3p^5 3d^6 4s^2\ ^6F\ ^6D\ ^4P$ lines at energies below the dominant $3p^6 3d^5 4s^2\ ^6S \rightarrow 3p^5 3d^6 4s^2\ ^6P$ resonance are missing in their spectrum.

Garvin et al. (1983) included the spin-orbit coupling in their MBPT calculation. They also extended the theoretical 3d cross section to energies above the $3p^5 3d^5 4s^2\ ^5P$ ionisation threshold. For the giant resonance in the 3d partial cross section the result agrees with those of Amusia et al. (1981) and with the experimental results (Bruhn et al. 1982; Kobrin et al. 1984; Krause et al. 1984). On the other hand they predicted prominent $3p^6 3d^5 4s^2 \rightarrow 3p^5 3d^5 4s^2$ ns, nd Rydberg series converging towards the $3p^5 3d^5 4s^2\ ^7P$ series limits which have only weak counterparts in the experimental spectra (Bruhn et al. 1978). Kelly (1983) speculated that photoionisation-with-excitation processes may be responsible for this discrepancy. The importance of these processes has been underlined by the recent results for the $3p^6 3d^5 4s^2 \rightarrow 3p^5 3d^5\ (^5P)\ 5s\ ^6P$ resonant transitions (Garvin et al. 1983b). In order to test these ideas we determined the resonant satellite photoemission in the photon energy range of the $3p \rightarrow 3d$, $3p \rightarrow nd$, ns transitions. In doing so we also greatly improved the data on the main photoemission lines and the corresponding partial cross sections.

II. Experiment

For the photoelectron measurements the synchrotron radiation emitted by the electron storage ring DORIS was monochromatized (bandwidth 0.15 eV at 40 eV and 0.3 eV at 65 eV) with a toroidal grating monochromator (Bruhn et al. 1983). The monochromatic photon beam (about 10^{11} photons/sec) was focused onto the interaction zone, where it crossed a beam of atomic Mn emanating from a resistively heated high temperature furnace. Of all 3d-metals Mn is the easiest to prepare as an atomic beam. Temperatures around 1200 K are sufficient to attain a vapour pressure in the 0.1 to 1 Pa range. This temperatures are still below the melting point, thus the reactive liquid state is avoided. The furnace could be operated up to 10 hours at reasonably constant conditions.

The kinetic energy of electrons emerging from the interaction zone was determined by a cylindrical mirror analyzer (angular acceptance 0.8 % of 4π, energy resolution ΔE = 0.8 % of the pass energy). Only electrons emitted at angles close to the magic angle of 54°44' relative to the polarization vector of the incoming light were accepted by the analyzer. This eliminates the influence of the asymmetry of the photoelectron angular distribution (Starace 1982; Samson 1982) and allows for a direct determination of partial cross sections. The partial cross sections were determined from a series

of photoelectron spectra taken at different photon energies and also from constant ionic final state spectra, where the photon energy and the pass energy of the electron energy analyzer are scanned simultaneously. All spectra were normalized to the incoming photon flux and corrected for the energy dependent bandpass of the electron spectrometer. Since the density of atoms in the interaction zone was not determined, only relative cross sections are given. Instabilities of the atomic beam, which is estimated to yield 10^{12} atoms/cm^3 in the interaction zone, are the main source of errors. Every cross section presented in this paper was derived from several independent runs. The count rates were up to 2000 cts/s for the main $3d^4(^5D)4s^2\varepsilon l$ line and typically 100 cts/s for the stronger satellites. The scatter of the data presented in Figs. 2-5 gives a good idea of the relative accuracy of the partial cross sections which we estimate to be 10 %. Details of the experimental set up are given elsewhere (Schmidt et al. 1984; Schröder 1982).

III. Results and Discussion

III.1 Photoelectron Spectra

A series of photoelectron spectra taken at different photon energies between 45 eV $\leq \hbar\omega \leq$ 55 eV are given in Fig. 1. The figure clearly shows the strong dependence of the intensity of the various photoemission lines on the photon energy. The main $3d^5 4s^2 \rightarrow 3d^5 4s\ \varepsilon l$, $3d^4 4s^2\ \varepsilon l$ lines ($E_B < 15$ eV) are strongly enhanced for photon energies between 49 eV and 52 eV due to the coupling of the continuum channels to the $3p^6 3d^5 4s^2\ ^6S \rightarrow 3p^5 3d^6 4s^2$ (^6P 50.0 eV $\pm$ 0.2 eV, ^4F 51.0 $\pm$ 0.2 eV) excitations. These lines also display a marked enhancement at $\hbar\omega$ = 48.1 eV, the position of the $3p^6 3d^5 4s^2\ ^6S \rightarrow 3p^5 3d^6 4s^2\ ^6D$ transition (Bruhn et al. 1978; Bruhn et al. 1982a). The dominant $3d^5 4s^2\ ^6S \rightarrow 3d^4 4s^2(^5D)\ \varepsilon l$ line is suppressed at $\hbar\omega$ = 47.5 eV due to the destructive interference between the $3p^6 3d^5 4s^2\ ^6S \rightarrow 3p^5 3d^6 4s^2\ ^6P$ channel and the $3p^6 3d^5 4s^2\ ^6S \rightarrow 3p^6 3d^4 4s^2\ (^5D)\ \varepsilon l$ channel. The $3d^5 4s^2 \rightarrow 3d^5 5s\ \varepsilon l$, $3d^4 4s\ nl\ \varepsilon l$ satellite lines are also enhanced for photon energies beween 49 eV and 52 eV. But in contrast to the main lines they show in part a marked enhancement in the region of the $3p^6 3d^5 4s^2 \rightarrow 3p^5 3d^5 4s^2$ nd, ns Rydberg transition (54 eV $\leq \hbar\omega \leq$ 57 eV). Our assignment of the photoemission lines is summarized in Table I. The assignment is based on the tabulated energy values (Corliss and Sugar 1977). We will come back to the assignment of the satellite lines later on.

III.2 Total cross sections and partial cross sections of the main lines

Theoretical background

The theoretical description of the resonant behaviour of total and partial cross sections when many resonances interfere via many autoionization and Auger decay channels is extremely complicated (Starace 1977; Combet-Farnoux 1982; Davis and Feldkamp 1981; Starace 1982; Wendin 1982 b). Therefore there are no simple parametrized expressions which could be used to describe the total cross sections and the partial cross sections. In order to simplify the situation we assume that the Mn spectra at the 3p threshold are dominated by the $3p^6 3d^5 4s^2\ ^6S \rightarrow 3p^5 3d^6 4s^2\ ^6P$ resonance. This brings us back to the case of one single resonance interacting with several continua. In this case the total cross section is given by (Fano 1961):

$$\sigma_t = \sigma_t^o \left[(1-\rho^2) + \rho^2 \frac{(q+\varepsilon)^2}{1+\varepsilon^2} \right] \qquad (1)$$

$$\varepsilon = \frac{E - E_o}{\Gamma/2}$$

where σ_t^o is the cross section far from resonance, Γ and E_o are the full-width at half-maximum and the position of the resonance, respectively, q is the asymmetry parameter and ε is the reduced energy. The partial cross section σ_μ in each channel μ is presented by

$$\sigma_\mu = \sigma_\mu^o \left[1 + |\alpha_\mu|^2 \frac{q^2+1}{\varepsilon^2+1} + 2\ \mathrm{Re}\alpha_\mu \frac{\varepsilon q - 1}{\varepsilon^2+1} + 2\ \mathrm{Im}\alpha_\mu \frac{\varepsilon+q}{\varepsilon^2+1} \right], \qquad (2)$$

where q and ε are the parameters defined for the total cross section (Combet-Farnoux 1982). The off-resonance partial cross section is given by σ_μ^o. The complex parameter α_μ can be interpreted as a measure of the coupling between the μ th channel and the resonance. For details the reader is referred to the literature (Combet-Farnoux 1982, Starace 1977). If the parameter α takes a finite value the above expression can be transformed into

$$\sigma_\mu = \sigma_\mu^o \left[(1 - \rho_\mu^2) + \rho_\mu^2 \frac{(q_\mu+\varepsilon)^2}{\varepsilon^2+1} \right] \qquad (3)$$

where ρ_μ and q_μ are effective Fano parameters. For α towards infinity the partial cross section displays a Lorentzian profile. The Fano parameters are assumed constant over the resonance.

Total cross section

The total cross section determined by summing the contributions of all photoemission channels is presented in the uppermost part of Fig. 2. The $3p^5 3d^5 4s^2\ ^7P_4$ (56.5 ± 0.2 eV), $^7P_3$ (57.1 ± 0.2 eV), $^7P_2$ (57.4 ± 0.2 eV) ionization potentials, determined from ejected electron spectra (Schmidt et al. 1984), are indicated by the vertical bars. For comparison the photoabsorption spectrum (Bruhn et al. 1978) is included. The absorption spectrum has been adjusted at energies below the onset of the 3p excitations. Furthermore the absorption spectrum has been scaled in order to make the amplitudes of the $3p \rightarrow 3d$ maximum of both curves match. Both spectra clearly show the $3p^6 3d^5 4s^2\ ^6S \rightarrow 3p^5 3d^6 4s^2\ ^6D$ transition at 48.1 eV. The dominant maximum at 50.4 eV is due to the $3p^6 3d^5 4s^2\ ^6S \rightarrow 3p^5 3d^6 4s^2\ ^6P$ excitation. The assignment is based on the energy positions, oscillator strengths and the calculations performed by Davis and Feldkamp (1978).

The maxima calculated by Davis and Feldkamp (1978) and by Garvin et al. (1983) both show a shoulder. But the calculations disagree in respect to the energy position and the assignment of the shoulder. According to the calculations of Garvin et al. (1983) the $3p^6 3d^5 4s^2\ ^6S \rightarrow 3p^5 3d^6 4s^2\ ^4F$ transitions are responsible for the peak at 50.9 eV whereas according to Davis and Feldkamp transitions to other ^4L final states contribute. Details of the structure in this region are sensitive to the location of the numerous energy levels, the amount of spin orbit interaction, and the strength of the interaction with the continua. The $3p^6 3d^5 4s^2\ ^6S \rightarrow 3p^5 3d^5 4s^2 ns,nd$ Rydberg transitions showing up between 54 eV and 57 eV in the absorption spectrum are hardly discernible in the total cross section obtained from the photoelectron spectra. The absorption spectrum overshoots the total cross section determined from the photoelectron spectra above 53 eV by a factor of two. This striking discrepancy probably rests with the difficulties encountered in determining reliable relative absorption cross sections from a series of photographically registered absorption spectra (Bruhn et al. 1978). In order to obtain the Fano parameters the total "photoelectron cross section" has been fitted by a Fano profile (equation 1) centered at the $3p^6 3d^5 4s^2 \rightarrow 3p^5 3d^6 4s^2\ ^6P$ transition. The $3p^6 3d^5 4s^2 \rightarrow 3p^5 3d^6 4s^2\ ^4F$ and the $3p^6 3d^5 4s^2\ ^6S \rightarrow 3p^5 3d^6 4s^2\ ^6D$ excitations have been taken into account by superimposing Lorentzian profiles. The instrumental broadening has been simulated by convoluting the Fano profile and the Lorentzian lines by a Gaussian of 0.18 eV FWHM. The parameters thus obtained are listed in Table II.

Partial cross sections of the main $3d^5 4s^2\ ^6S \rightarrow 3d^4 4s^2\ ^5D\varepsilon l$, $3d^5 4s\ ^{5,7}S\varepsilon l$ photoemission lines

The center part of Fig. 2 gives the $3d^5 4s^2\ ^6S \rightarrow 3d^4 4s^2\ ^5D\varepsilon l$ partial cross section. As for the total cross section the experimental spectrum can be approximated by the superposition of a Fano type profile (equation 3) and a Lorentzian profile. The effective parameters are given in Table II. We note that Kobrin et al. (1984), guided by the photoabsorption spectrum (Bruhn et al. 1978) arrived at a similar fit for the main 3d-photoemission cross section, although experimentally they did not resolve the overlapping resonances. For comparison the spectrum calculated by Garvin et al. (1983a) is also shown in Fig. 2. For energies above 50 eV spin-orbit effects have not been taken into account by the theory. For the dominant maximum the spectrum calculated by Amusia et al. (1981) (not shown in Fig. 2) is in good agreement with the theoretical spectrum shown in Fig. 2. Including spin-orbit effects up to 53 eV Garvin et al. (1983a) obtained a somewhat lower absorption cross section at the maximum and a shoulder at the high energy side (curve not included in Fig. 2). All spectra have been adjusted at 45 eV i.e. below the onset of the 3p excitations. The gross features of the experimental spectrum are reproduced by the theoretical spectra. The effective q values (exp. 2.5 $\pm$ 0.2, theor. 2.5) agree whereas the theoretical Γ value (2 eV) is larger than the experimental one (1.34 $\pm$ 0.10). The RPAE calculation (Amusia et al. 1981) does not give any fine structure. In contrast to this the MBPT calculation (Garvin et al. 1983a) predicts sharp lines at the 3p threshold and sharp Rydberg lines in the region of the weak structures of the absorption spectrum. The marked discrepancies between experiment and theory are:

(i) the position of the sharp lines at the 3p threshold differ from those determined experimentally,

(ii) instead of sharp Rydberg lines the experimental spectrum displays only weak structures.

In respect of the first point it is interesting to note that the semiempirical calculations of Davis and Feldkamp (1978) give a good description of the sharp lines at the 3p threshold (Bruhn et al. 1978, 1982a). The second point can be traced back to the neglect of photoionization-with-excitation in the MBPT calculations. This will be made clear in context with the discussion of the satellite partial cross sections. The asymmetric Fano type profile of the big resonance in the total cross section and the $3d^5 4s^2\ ^6S \rightarrow 3d^4 4s^2 (^5D)\varepsilon l$ partial cross section proves the interference between this ionization channel and the $3p^6 3d^5 4s^2\ ^6S \rightarrow 3p^5 3d^6 4s^2\ ^6P$ excitation mediated via autoionization of the ^6P state.

The $3d^5 4s^2\ ^6S \rightarrow 3d^5 4s\ ^{5,7}S\varepsilon l$ partial cross section can be fitted by a Lorentzian line shape, if one ascribes the deviations at the low energy side to the contribution of the discrete transitions below the $^6S \rightarrow {}^6P$ resonance (bottom part of Fig. 2). The experimental data, especially the constant ionic final state spectrum renders this unlikely, because it does not display a superposition of narrow profiles. A good approximation of the experimental data over the whole energy range can be achieved by a Fano profile with $q = -8$. A close scrutiny of the $3p^6 3d^5 4s^2\ ^6S \rightarrow 3p^5 3d^6 4s\ ^{5,7}S\varepsilon l$ partial cross section published by Garvin et al. (1983a) (see Fig. 2), though considerably lower, reveals a similar weak asymmetry. This means that the $3p^5 3d^6 4s^2 \rightarrow 3p^6 3d^5 4s\varepsilon l$ decay is only weakly modified by interference with the $3d^5 4s^2 \rightarrow 3d^5 4s\varepsilon l$ ionization due to the small cross section for this process. The line parameters obtained by the fits of both partial cross sections (see Table II) are in agreement with those obtained by a model calculation taking the coupling of the $3p^5 3d^6 4s^2\ ^6D$, ^6P states with the $3d^5 4s\ ^{5,7}S\varepsilon l$, $3d^4 4s^2\ ^5D\varepsilon l$ continua into account (Bruhn et al. 1982a). This adds to the confidence in the simple approach.

The branching ratio $\sigma(3d^5 4s\ ^7S\varepsilon l)/\sigma(3d^5 4s\ ^5S\varepsilon l)$ drops from a value of 0.8 $\pm$ 0.1 at 44 eV to a minimum value of 0.25 $\pm$ 0.03 between 50 eV and 51 eV. Towards higher energies it rises again, reaching 0.8 $\pm$ 0.2 at 54 eV. Krause et al. (1984) determined this branching ratio over a wider energy range. In the region of overlap there is fair agreement between both sets of data, though our minimum value lies somewhat above their value of 0.19 $\pm$ 0.06.

III.3 Partial cross sections of satellite lines

Partial cross section of the $3d^5 4s^2\ ^6S \rightarrow 3d^5(^4G, {}^4F) 4s\ ^5G, {}^5F\varepsilon l$ recoupling satellites

Dyke et al. (1979) detected seven satellite lines between 9 and 13 eV binding energy in their HeI photoelectron spectrum of atomic Mn. Close to the $3p \rightarrow 3d$ resonance four of these lines plus an additional line at 11.2 eV binding energy show up in our spectra (Bruhn et al. 1982a, see Fig. 1).

In contrast to the 4s-lines discussed above the remaining $3d^5$ electrons of the ion are coupled to a ^4L state. In Fig. 3 the partial cross sections

of the $3d^5 4s^2\ ^6S \rightarrow 3d^5(^4F)4s\ ^5F\varepsilon l$, $3d^5(^4G)4s\ ^5G\varepsilon l$ photoemission lines are presented for photon energies between 45 eV and 55 eV. Both cross sections are enhanced at the energies of the $3p^6 3d^5 4s^2\ ^6S \rightarrow 3p^5 3d^6 4s^2\ ^6D$ (48.1 eV), ^4P (48.5; 48.8 eV), ^6P (50.0 eV), ^4F (51.0 eV) excitations (Bruhn et al. 1978; Davis and Feldkamp 1978). In the range of the strong resonances the experimental points can be approximated by a superposition of three Lorentzian curves centered at the $^6S \rightarrow {}^6D$, ^6P, ^4F transitions. The instrumental broadening of our set-up is important for the $^6S \rightarrow {}^6D$ resonance, which has a FWHM of ≤ 0.1 eV in the absorption spectrum (Bruhn et al. 1978). The fit parameters are summarized in Table II. The symmetric line shapes signal the weakness of the interference between the closed and open channels. This is consistent with the small $3d^5 4s^2\ ^6S \rightarrow 3d^5 4s\ (^5F, {}^5G)\varepsilon l$ ionization cross section outside the resonance shown in Fig. 1. The $3d^5 4s^2\ ^6S \rightarrow 3d^5 4s\ ^5D\varepsilon l$ photoemission line (E_B = 11.5 eV) (see Fig. 1) is mainly driven by the $3p^6 3d^5 4s^2\ ^6S \rightarrow 3p^5 3d^6 4s^2\ ^6D$ excitation, indicating a small $3p^5 3d^6 4s^2\ ^6P \rightarrow 3p^6 3d^5 4s\ ^5D\ \varepsilon l$ decay rate.

Partial cross section of the $3d^5 4s^2\ ^6S \rightarrow 3d^5 5s\ ^5S\varepsilon l$ two electron satellite line

The photoemission line (E_B = 16.8 eV) popping up at $\hbar\omega$ = 50.6 eV (see Fig. 1) is still puzzling us. According to Corliss and Sugar (1977) only the MnII $3d^5(^6S)5s\ ^{7,5}S$ and $3d^5(^4D)4p\ ^3P$ states have the correct binding energies. The partial cross section of this line (Fig. 4) can be well approximated by a Lorentzian convoluted by a Gaussian. There seems to be a weak coupling to the $3p^6 3d^5 4s^2\ ^6S \rightarrow 3p^5 3d^6 4s^2\ ^4L$ transitions located between 49 eV and 50 eV. The half-width of the Lorentzian (0.34 eV) is close to the half-width for the $3p^6 3d^5 4s^2\ ^6S \rightarrow 3p^5 3d^6 4s^2\ ^4F$ excitation. This leads us to the conclusion that this line is driven by a $^6S \rightarrow {}^4X$ transition, where X stands for P, D, F. Based on this we can exclude the MnII $3d^5(^6S)5s\ ^7S$ final state, because it cannot couple to a ^4X state with the outgoing electron. Therefore in LS-coupling the decay rate would be zero. There are several $3d^5 4s^2\ ^6S \rightarrow 3d^5(^4X)4p\varepsilon l$ photoemission lines spanning the binding energy range from 15.4 eV to 17.7 eV (see Fig. 1). The partial cross section for this group of lines except for the peculiar line at E_B = 16.8 eV resembles that of the $3d^4(^5D)4s4p$ shake up line (see below). Since it is hard to see why just one of the $3d^5 4s^2\ ^6S \rightarrow 3d^5(^4D)4p\ ^3P\varepsilon l$ shake up lines should be enhanced so dramatically we tend to ascribe this line to the $3d^5(^6S)5s\ ^5S\varepsilon p\ ^6P$, $\varepsilon f\ ^6F$ final state. LS-coupling favours the resonant enhancement via $3p^6 3d^5 4s^2\ ^6S \rightarrow 3p^5 3d^6 4s^2\ ^4P$, ^4F excitations.

Partial cross section of the $3d^5 4s^2\ ^6S \rightarrow 3d^4(^5D)4s4p$, 4d, $5s\varepsilon l$ two electron satellites

The assignment of the $3d^5 4s^2\ ^6S \rightarrow 3d^4(^5D)4s4p\varepsilon l$, $3d^4(^5D)4s5s\varepsilon l$, $3d^4(^5D)4s4d\varepsilon l$ photoemission lines is based on the tabulated energy values for atomic Mn (Corliss and Sugar 1977), the ordering of the isoelectronic states of atomic Cr (Sugar and Corliss 1977) and the energies calculated for the Mn $3p^6 3d^5 4s^2 \rightarrow 3p^5 3d^5 4s^2 5s$, 4d Rydberg transitions (Garvin et al. 1983a). The partial cross sections for these photoemission channels are presented in Fig. 5. All lines are enhanced in the range of the $3p^6 3d^5 4s^2\ ^6S \rightarrow 3p^5 3d^6 4s^2\ ^6P$, ^4F excitations. We can approximate the partial cross sections in this photon energy range by the superposition of a Fano type profile and a Lorentzian profile. From the effective q and Γ values (see Table II) we conclude that there is considerable interference between the discrete closed $^6S \rightarrow {}^6P$ channel and the ionization-with-excitation channels. In contrast to all partial cross sections discussed so far there is a further resonant enhancement in the region of the Rydberg transitions. A detailed analysis is hampered by the limited energy resolution of our set-up (0.2 eV at 55 eV). Inspite of this the spectra yield enough information for a tentative assignment. The maxima positioned at 54.4 $\pm$ 0.2 eV, 54.9 $\pm$ 0.2 eV and 55.3 $\pm$ 0.2 eV in the center spectrum of Fig. 5 are ascribed to the following photoionization and decay sequence: $3p^6 3d^5 4s^2\ ^6S \rightarrow 3p^5 3d^5 4s^2(^7P_{4,3,2})5s \rightarrow 3p^6 3d^4 4s5s\varepsilon l$. In analogy we assign the maximum positioned at 55.3 $\pm$ 0.2 eV in the upper curve of Fig. 5 to the $3p^6 3d^5 4s^2\ ^6S \rightarrow 3p^5 3d^5 4s^2\ (^7P_4)4d$ photoexcitation decaying into $3p^6 3d^4(^4D)4s4d\varepsilon l$. These decay channels, not taken into account by the MBPT calculations (Garvin et al. 1983), result in a broadening of the Rydberg lines and thus explain the missing of sharp Rydberg lines in the experimental spectra (see Fig. 1). Also the $3p^5 3d^5 4s^2 nl \rightarrow 3p^6 3d^3 4s^2 nl\varepsilon l$ Auger decay may contribute to the broadening (see Garvin et al. 1983b) but from the ejected electron spectrum (Schmidt et al. 1984) we know that the $M_{23} - M_{45}N_1$ Auger transition rate is much larger than the $M_{23} - M_{45}M_{45}$ rate. In LS-coupling the $M_{2,3}M_{4,5}M_{4,5}$ Auger transition is forbidden by selection rules. In the photon energy range of the ^7P ionization thresholds the partial cross sections of all two electron satellites display structures which turn into a pronounced peak for the $3d^4(^5D)4s4p\varepsilon l$ emission (see Fig. 5). The enhanced satellite emission in this energy range (see also below) corresponds to the broad absorption maximum above 56 eV shown in Fig. 1.

The dramatic changes of the satellite photoemission spectrum when tuning the photon energy across the $3p^5 3d^5 4s^2\ ^7P_{2,3,4}$ ionization thresholds are shown in Fig. 6. In addition to the lines discussed above (lines 1-6, see Table 1) new lines (A-F) pop up in this energy range. The binding energies are listed in Table 3. For photon energies above the highest $^7P_2$ (57.4 eV) ionization limit the $M_{2,3}$, $M_{4,5}$, N_1 Auger lines are discernible.

The asymmetric line shape indicates the influence of post-collision interaction (see e.g. Schmidt 1982). The kinetic energies of the Auger electrons determined from the photoemission spectrum (26.6 ± 0.2 eV, 27.2 ± 0.2 eV, 27.6 ± 0.2 eV) are approximately 1 eV higher than those obtained for excitations high above threshold (25.63 ± 0.2 eV), 26.16 ± 0.2 eV, 26.5 ± 0.2 eV) (Schmidt et al. 1984). This is consistent with the expected energy gain for the Auger electrons by post-collision interaction. Lowering the photon energy results in the disappearance of the Auger lines and in an increase of the intensity of lines A-F, because the slow 3p-photoelectron is captured in a bound orbital (shake down) leading to MnII $3d^4 n(n'l')$ final states. These states can also be reached by ionization and simultaneous excitation. In this context we want to refer the reader to the discussion of the connection between Auger lines, resonant satellite lines and post collision interaction for the 3p threshold region of atomic Ca. (Wendin 1982 a,b; Bizau et al. 1984).

No marked changes of the photoemission spectrum (10 eV < E_B < 35 eV) have been detected for photon energies between 68 eV and 72 eV. According to Garvin et al. (1983b) $3p^6 3d^5 4s^2\ ^6S \rightarrow 3p^5 3d^5 (^5P) 4s^2 5s$ transitions broadened by the coupling to the $3p^6 3d^5 4s^2\ ^6S \rightarrow 3p^6 3d^3 (^4F) \in f (^5P) 4s^2 5s\ ^6P$ photoionization with excitation give rise to noticeable maximum in the absorption spectrum at 71.4 eV. The energy calculated for the $3p^5 3d^5 4s^2\ ^5P$ ionization limit is 74.1 eV.

Conclusions

The general features of the resonances in the total cross section and the partial cross section of the main photoemission channels are fairly well described by recent MBPT and RPAE calculations. However, a closer look at the data reveals marked discrepancies between theory and experiment which in many cases can be traced back to the neglect of satellite emission channels in the theoretical treatments. Our results clearly demonstrate the importance of ionization with excitation.

Acknowledgement

The authors thank the HASYLAB staff for the continuous support. The research was sponsored by the Bundesministerium für Forschung und Technologie.

Table 1

Experimental binding energies E_B of the states of MnII giving rise to the photoemission lines in Fig. 1. The tabulated binding energy of the $3d^5(^6S)$ $4s\ ^7S_3$ state has been used as reference.

Line No.	E_B (eV)	State of MnII
1	25.1 ± 0.2	$3d^4(^5D)4s\ 4d$
2	24.2 ± 0.2	$3d^4(^5D)4s\ 5s$
3	20.8 ± 0.2	$3d^4(^5D)4s\ 4p\ (^5P)$
4	20.6 ± 0.2	$3d^4(^5D)4s\ 4p\ (^5F)$
5	16.8 ± 0.2	$3d^5(^6S)5s\ ^5S$
	15.4 - 17.7	$3d^5(^4X)4p\ ^5X$
6	14.2 ± 0.15	$3d^4(^5D)4s^2\ ^5D$
7	12.8 ± 0.1	$3d^5(^4F)4s\ ^5F$
8	11.5 ± 0.1	$3d^5(^4D)4s\ ^5D$
9	11.2 ± 0.1	$3d^5(^4P)4s\ ^5P$
10	10.8 ± 0.1	$3d^3(^4G)4s\ ^5G$
11	9.3 ± 0.1	$3d^6(^5D)\ ^5D$
12	8.6 ± 0.05	$3d^5(^6S)4s\ ^5S$
13	7.44	$3d^5(^6S)4s\ ^7S$

Table 2

Fit parameters obtained for the total and partial cross sections in the photon energy range of the $3p^6 3d^5 4s^2\ ^6S \rightarrow 3p^5 3d^6 4s^2\ ^6D$, ^6P, ^4L excitations. The instrumental broadening has been taken into account by convoluting the profiles by a Gaussian of 0.18 eV FWHM. E_o is the resonance energy, Γ the full width at half maximum and q the asymmetry parameter. The Fano type profile for finite q turns into a Lorentzian for q towards infinity. The relative strength of the resonant part of the cross section is given by $f = \sigma_o \rho^2$. For the $^6S \rightarrow {}^6D, {}^4F$ excitations for which the partial cross sections and the total cross section display the same Lorentzian line shape, the relative strengths of the partial cross sections nicely add up to the strength of the total cross section. This is not expected to hold for the $^6S \rightarrow {}^6P$ excitation where the partial cross sections display different profiles. There is only a weak nonresonant background, most noticeable for the total cross section and the MnII $3d^5 4s\ ^5S+^7S$ partial cross section. Last digit errors are bracketed.

MnII final state	$^6S \rightarrow {}^6D$			$^6S \rightarrow {}^6P$			$^6S \rightarrow {}^4L\ (^4F)$					
	E_o(eV)	Γ(eV)	f	E_o(eV)	q	Γ(eV)	f	E_o(eV)	Γ(eV)	f	E_o(eV)	Γ(eV)	f
total cross section	48.2(1)	0.10(3)	0.34	50.1(1)	2.5(2)	1.3(1)	22.8				51.1(1)	0.5(1)	1.8
$3d^4(^5D)4s^2\ ^5D$	48.2(1)	0.10(3)	0.08	50.1(1)	2.5(2)	1.34(10)	18.6				51.1(1)	0.45(10)	1.3
$3d^4(^5D)4s\ 4p$				50.0(1)	2.2(1)	1.54(15)	0.85				51.2(2)	0.5(1)	0.05
$3d^4(^5D)4s\ 5s$				50.0(1)	2.1(1)	1.32(10)	0.66				50.9(1)	0.40(5)	0.06
$3d^4(^5D)4s\ 4d$				50.2(1)	2.2(1)	1.34(10)	0.35				51.2(2)	0.6(1)	0.05
$3d^5(^4F)4s\ ^5F$	48.2(1)	0.10(3)	0.21	50.2(1)		1.2(1)	0.63				51.0(1)	0.55(10)	0.21
$3d^5(^4G)4s\ ^5G)$	48.2(1)	0.10(3)	0.08	50.1(1)		1.3(1)	0.50				51.0(1)	0.6(1)	0.16
$3d^5(^6S)4s\ ^5S+^7S$				50.1(1)	-8(1)	1.7(1)	3.6						
$3d^5(^6S)5s\ ^5S$								50.60(5)	0.34(3)	0.77			

Table 3

Experimental binding energies of the additional lines (see Fig. 6). The binding energy of the $3d^4 4s5s\varepsilon l$ line (see Table 1) has been used as reference.

Line	E_B (eV)
A	29.4 ± 0.1
B	28.6 ± 0.1
C	27.4 ± 0.1
D	26.3 ± 0.1
E	22.5 ± 0.2
F	18.9 ± 0.2

References

Amusia M Ya, Ivanov V K and Chernysheva L V 1981a J. Phys. B14 L19

Amusia M Ya, Chernysheva L V and Sheftel S I 1981b Journ. Techn. Fiz 51 2411

Amusia M Ya 1983 Atomic Physics 8 ed. I. Lindgren, A. Rosén and S. Svanberg Plenum Press New York page 287 and references therein

Amusia M Ya, Dolmatov V K and Ivanov V K 1983 J. Phys. B16 L753

Bizau J M, Gérard P, Wuilleumier F J and Wendin G 1984 to be published

Bruhn R, Sonntag B and Wolff H W. 1978 Phys. Lett 69A 9

Bruhn R, Schmidt E, Schröder H and Sonntag B 1982a Phys. Lett. 90A 41

Bruhn R, Schmidt E, Schröder H and Sonntag B 1982b J. Phys. B15 2807

Bruhn R, Schmidt E, Schröder H, Sonntag B, Thevenon A, Passereau G and Flamand J 1983 Nucl. Instr. Meth. 208 771

Combet-Farnoux F and Ben Amar M 1980 Phys. Rev. A21 1975

Corliss Ch and Sugar J 1977 J. Phys. Chem. Ref. Data 6 1253

Crasemann B and Wuilleumier F 1984 in Atomic Inner-Shell Physics ed. B. Crasemann Plenum Publ. Corporation (to be published) and references therein

Davis L C and Feldkamp L A 1976 Solid State Comm. 19 413

Davis L C and Feldkamp L A 1977 Phys. Rev. B15 2961

Davis L C and Feldkamp L A 1978 Phys. Rev. A17 2012

Davis L C and Feldkamp L A 1981 Phys. Rev. B23 6239

Davis L C and Feldkamp L A 1983 private communication

Dyke J M, Fayad N K, Morris A and Trickle I R 1979 J. Phys. B12 2985

Fano U 1961 Phys. Rev. 124 1866

Garvin L J, Brown E R, Carter S L and Kelly H P 1983a J. Phys. B16 L269

Garvin L J, Brown E R, Carter S L and Kelly H P 1983b J. Phys. B16 L643

Kelly H P 1983 Atomic Physics 8 ed. I. Lindgren, A. Rosén and S. Svanberg, Plenum Press New York page 305 and references therein

Kobrin P H, Becker U, Truesdale C M, Lindle D W, Kerkhoff H G and Shirley D A 1984 J. Electron Spectrosc. Relat. Phenom. (to be published)

Krause M O, Carlson T A and Fahlmann A 1984 Phys. Rev. A (to be published)

Samson A F 1982 Handbuch der Physik vol. 31 123 and references therein

Schmidt E, Schröder H, Sonntag B, Voss H and Wetzel H E 1983 J. Phys. B16 2961

Schmidt E. Schröder H, Sonntag B, Voss H and Wetzel H E 1984 J. Phys. B17, 707

Schmidt V 1982 in X-Ray and Atomic Physics ed. B. Crasemann American Inst. of Phys. New York p. 544

Schröder H 1982 Thesis University of Hamburg

Starace A F 1977 Phys. Rev. A16 231

Starace A F 1982 Handbuch der Physik vol. 31 1 and references therein

Sugar J and Corliss Ch 1977 J. Phys. Chem. Ref. Data 6 317

Wendin G 1982a in X-Ray and Atomic Inner-Shell Physics 1982 ed. B. Crasemann Conference Proceedings no 94 American Institute of Physics New York page 495 and references therein

Wendin G 1982b Lecture Notes for the Summer School "New Trends in Atomic Physics" Les Houches and references therein

Zangwill A 1983 Atomic Physics 8 ed. I. Lindgren, A. Rosén and S. Svanberg Plenum Press New York page 305 and references therein

Figure Captions

Figure 1 Photoelectron spectra of atomic Mn. The photon energies at which the different spectra were recorded are given on the lefthand scale.

Figure 2 Upper part: Total photoionization cross section determined from the photoelectron spectra (full dots) and experimental absorption spectrum of atomic Mn (dash-dotted line, Bruhn et al. 1978). The solid line represents our fit from Table 2 convoluted by a Gaussian of 0.18 eV FWHM.
Center part: Partial $3d^5 4s^2\ ^6S \rightarrow 3d^4 4s^2(^5D)\varepsilon l$ cross section. Experiment: the full dots were derived from individual photoelectron spectra. The dashed curve was obtained by the constant ionic final state (CIS) method (see text). Theory: solid line from Garvin et al. 1983a (for discussion see part III.2).
Bottom part: Partial $3d^5 4s^2\ ^6S \rightarrow 3d^5 4s(^{5,7}S)\varepsilon l$ cross section. Experiment: full dots and dashed CIS-spectrum. Theory: Lower solid curve from Garvin et al 1983a. The upper solid curve represents the fit by a slightly asymmetric Fano profile, the parameters of which are given in Table 2.

Figure 3 Experimental $3d^5 4s^2\ ^6S \rightarrow 3d^5 4s(^5F,\ ^5G)\varepsilon l$ partial cross sections (full dots) fitted by a superposition of three Lorentzians convoluted by a Gaussian of 0.18 eV FWHM (instrumental resolution). Data from two different series of photoelectron spectra have been joined at the broad maximum. This is responsible for the scatter of the data points in this range. The better series of the photoelectron spectra convincingly displayed the double-peak structure, apparent in the fitted curves near 50 eV.

Figure 4 Experimental $3d^5 4s^2\ ^6S \rightarrow 3d^5 5s(^5S)\varepsilon l$ partial cross section. The full dots were derived from discrete photoelectron spectra for which a background correction could be performed. This could not be done for the CIS-spectrum (dashed curve) which therefore lies above the dots on the low energy slope. Both data sets indicate a weak enhancement near 49.6 eV. The solid line gives the approximation of the data by a Lorentzian (0.34 eV FWHM) convoluted by a Gaussian (0.18 eV FWHM).

Figure 5 Experimental $3d^5 4s^2\ ^6S \rightarrow 3d^4(^5D)4s4d\varepsilon l$, $3d^4(^5D)4s5s\varepsilon l$ and $3d^4(^5D)4s4p\varepsilon l$ partial cross sections. Approximation of the data by a superposition of a Fano type profile and a Lorentzian (solid line). The fitted curve fails to describe the strong enhancement in the range of the $3d^6 3d^5 4s^2\ ^6S \rightarrow 3p^5 3d^5 4s^2(^7P)nl$ Rydberg transitions between 54 eV and 57 eV. In a CIS-spectrum of the $3d^4(^5D)4s5s\varepsilon l$ channel several of the Rydberg transitions are clearly resolved (dashed line).

Figure 6 Post-collision interaction effects in a series of photoelectron spectra taken at photon energies close to the ^7P thresholds.

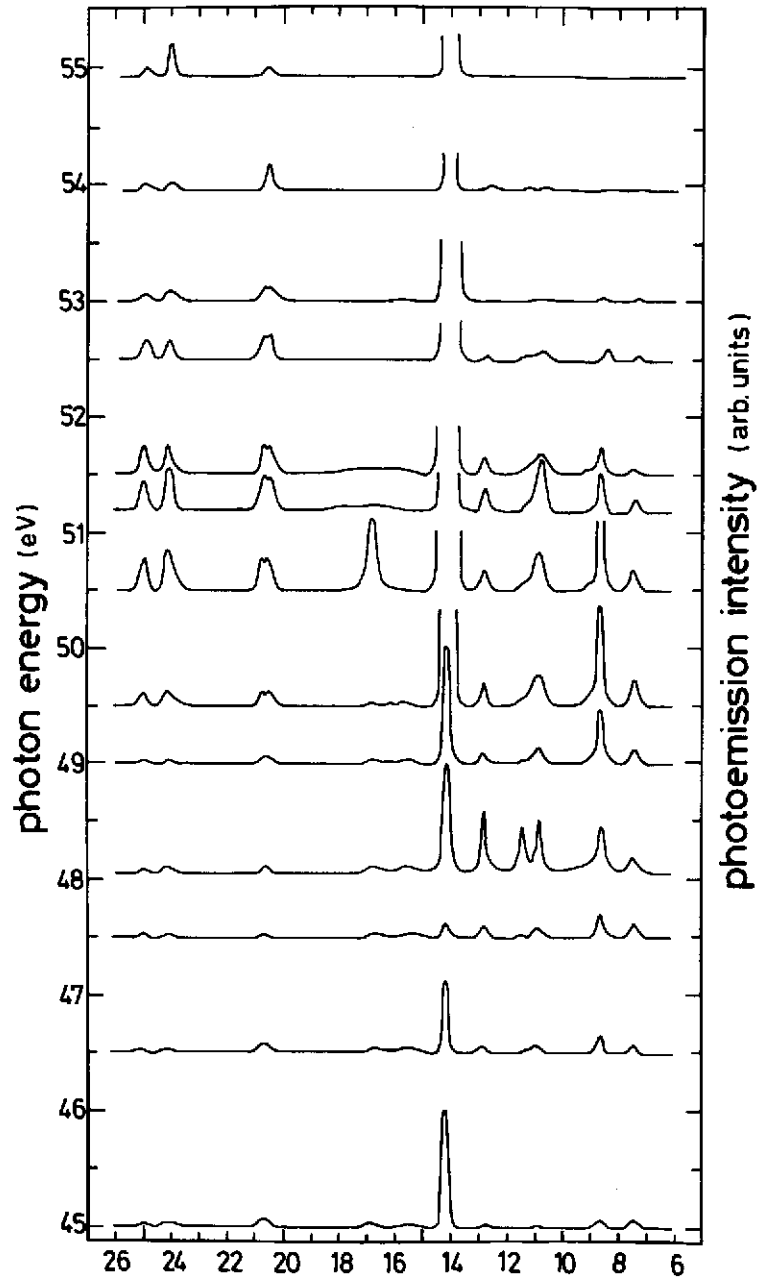

Fig. 1

36503

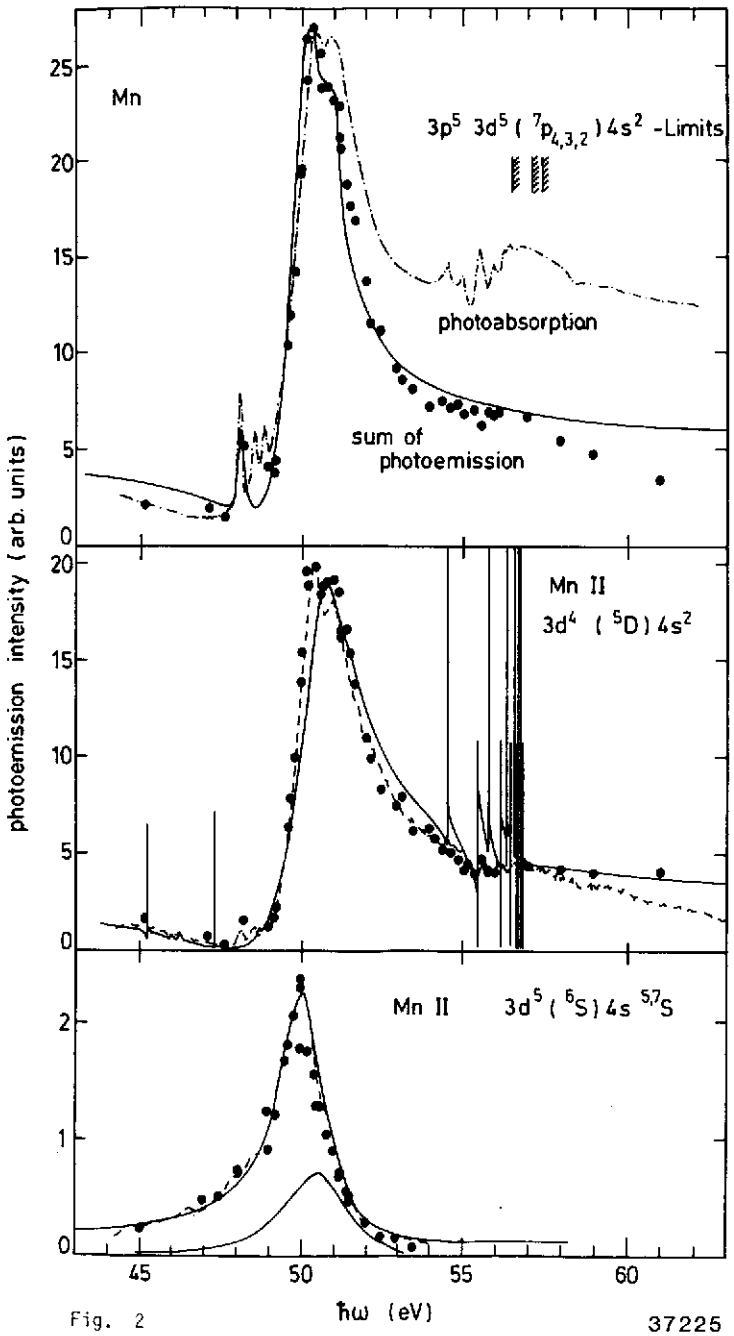

Fig. 2

37225

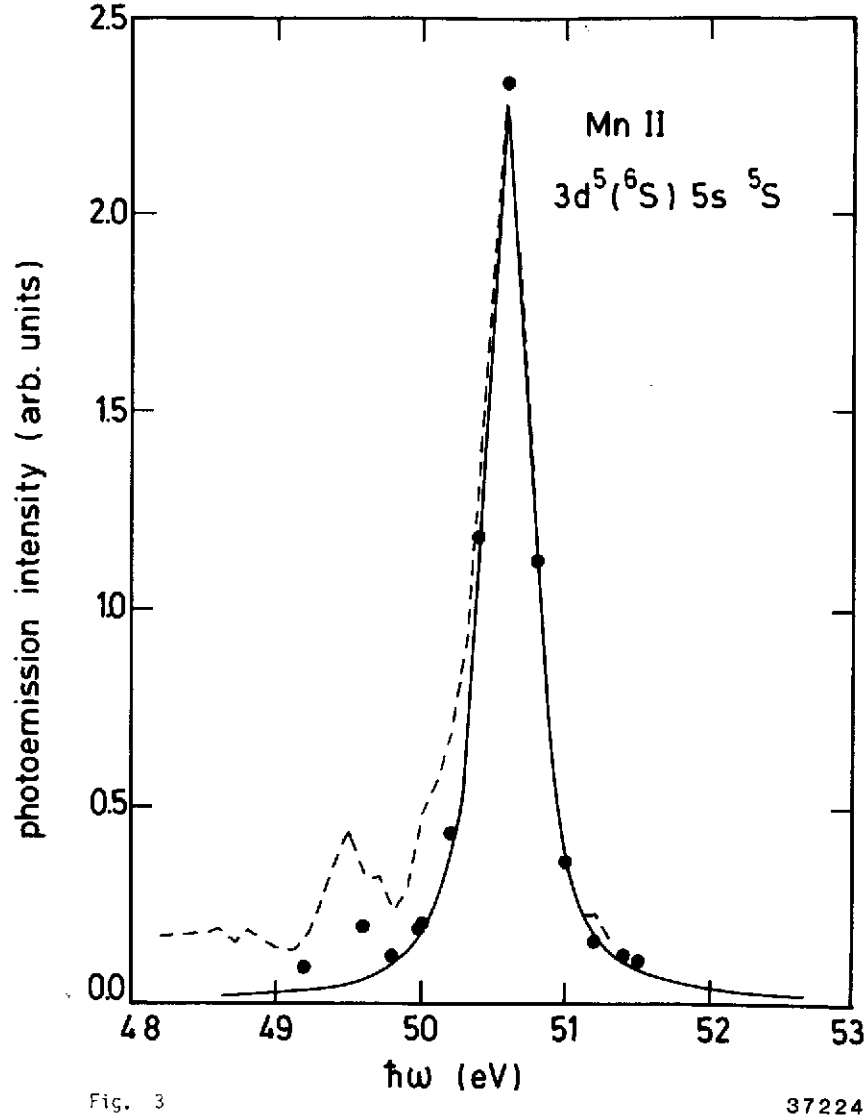

Fig. 3

37224

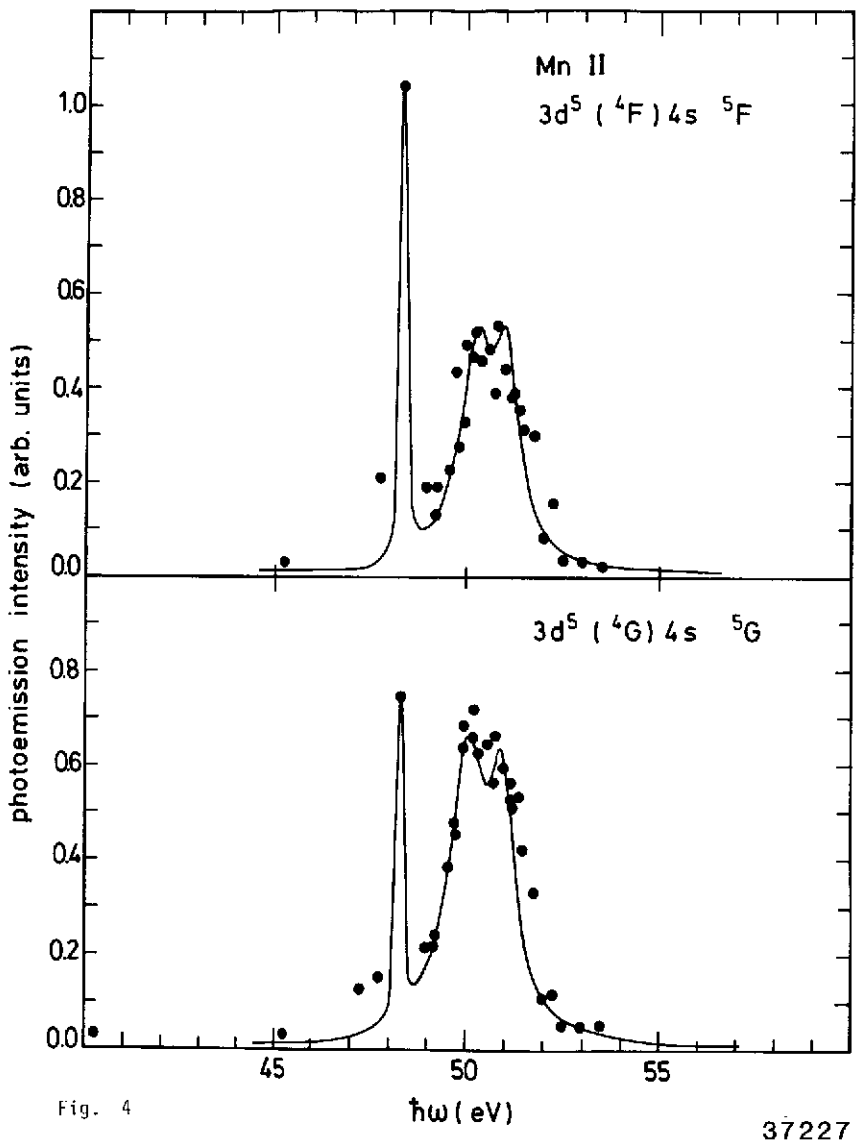
Mn II
3d5 (4F) 4s 5F
3d5 (4G) 4s 5G
photoemission intensity (arb. units)
ħω (eV)
37227

Fig. 4

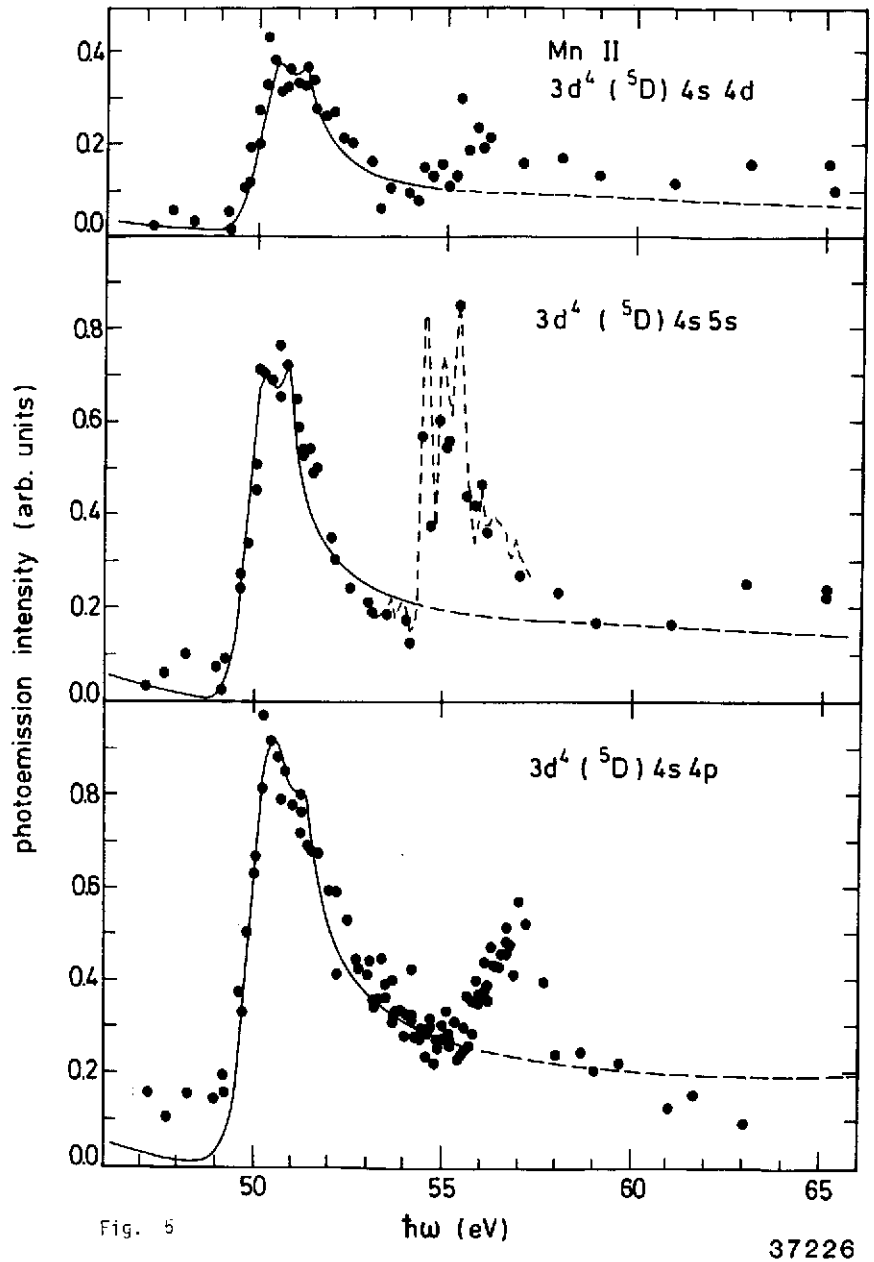
Mn II
3d4 (5D) 4s 4d
3d4 (5D) 4s 5s
3d4 (5D) 4s 4p
photoemission intensity (arb. units)
ħω (eV)
37226

Fig. 5

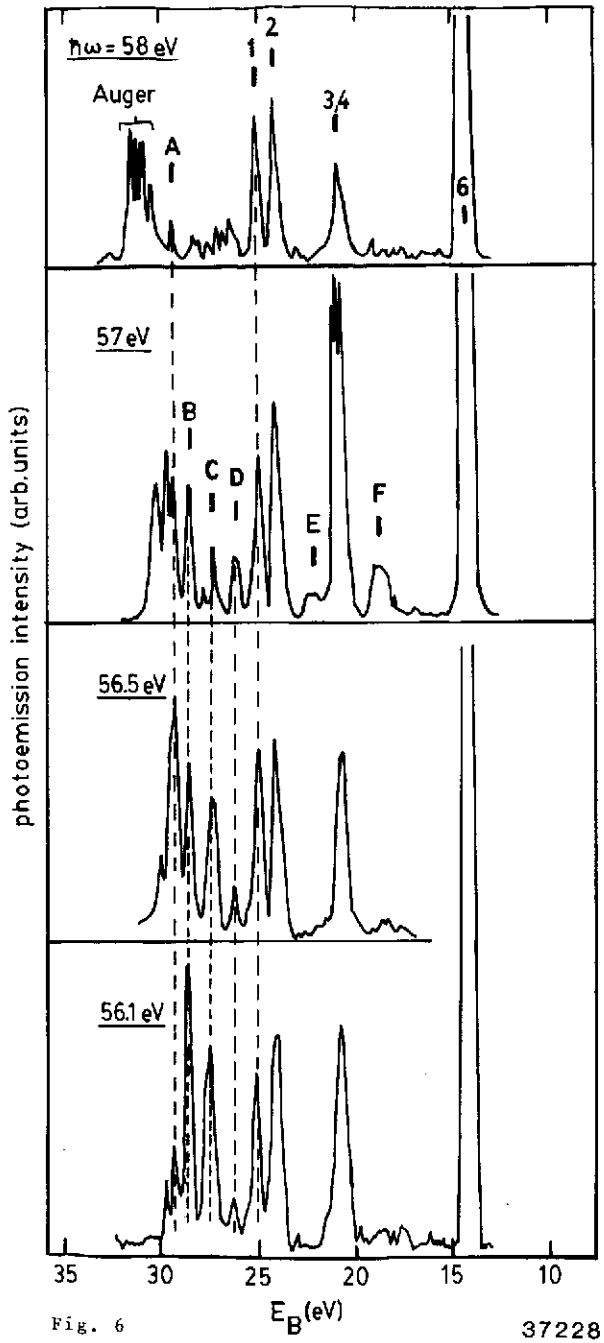
ħω = 58 eV
Auger
A
1
2
3,4
6
57 eV
B
C
D
E
F
56.5 eV
56.1 eV
photoemission intensity (arb.units)
35
30
25
20
15
10
E_B(eV)
37228

Fig. 6